ADVANCED FUNCTIONAL MATERIALS
www.afm-journal.de

Polymers of Intrinsic Microporosity Containing [2.2]Paracyclophane Moieties: Synthesis and Gas Sorption Properties

Yuting Li, Julian Brückel, Marjan Jereb, Anže Zupanc, Sami-Pekka Hirvonen, Sami Hietala, Marianna Kemell, Yue Wu, Olaf Fuhr, Ross D. Jansen-van Vuuren, Mariolino Carta,* and Stefan Bräse**

The unique structure of [2.2]paracyclophane (PCP) with its rigidity, stability, and planar chirality has gained significant attention in polymer and material research. In this work, the incorporation of amino-functionalized PCPs within polymers of intrinsic microporosity (PIMs) is reported for the first time. Three different PCP-PIMs were prepared via a Tröger's base formation mechanism, and their structures characterized via solid-state NMR, MALDI-TOF, and SEM. Their porosity was evaluated using gas adsorption (N_2 and CO_2) based on theoretical calculations such as Brunauer–Emmett–Teller (BET), NLDFT pore size distribution (PSD) and ideal IAST CO_2/N_2 selectivity (15/85), a crucial separation when considering the capture of CO_2 from flue gas. The surface areas were found to be between 200–230 $m^2\ g^{-1}$ while the selectivity for CO_2/N_2 ranged from 46 to 70.

1. Introduction

[2.2]Paracyclophane (PCP) consists of two benzene rings connected via two ethylene bridges at positions 1 and 4, creating strain within the molecule. However, due to the lack of free rotation of the aromatic rings, PCP is more stable than expected[1] and presents planar chirality.[2] PCPs have therefore been explored as building blocks for the supramolecular assembly of Metal–Organic Frameworks (MOFs)[3] and monomers for the synthesis of polymers for various applications, mainly to exploit their propensity to form rigid and layered structures.[4]

In this work, we describe for the first time, the synthesis and evaluation of polymers of intrinsic microporosity (PIMs) in which PCP units have been incorporated. PIMs represent a relatively new class of functional materials.[5] Their porosity arises from the appropriate choice of rigid and contorted building blocks (monomers) that prevent the efficient packing of the polymer chains, ultimately resulting in the formation of micro- and nano-pores.[6]In recent years, PIMs have emerged as excellent materials for applications such as gas separation membranes,[7] gas storage,[8] coating of electrodes for electrochemical reactions,[9] water purification,[10] and catalysis.[11] For example, PIMs have demonstrated great efficiency in separating

Y. Li, J. Brückel, S. Bräse
Institute of Organic Chemistry (IOC)
Karlsruhe Institute of Technology (KIT)
Kaiserstraße 12, 76131 Karlsruhe, Germany
E-mail: stefan.braese@kit.edu

M. Jereb, A. Zupanc, R. D. Jansen-van Vuuren
Faculty of Chemistry and Chemical Technology
University of Ljubljana
Večna pot 113, Ljubljana 1000, Slovenia
E-mail: Ross.JansenvanVuuren@fkkt.uni-lj.si

A. Zupanc, S.-P. Hirvonen, S. Hietala, M. Kemell
Department of Chemistry
Faculty of Science
University of Helsinki
A. I. Virtasen aukio 1, Helsinki 00014, Finland

Y. Wu, M. Carta
Department of Chemistry
Faculty of Science and Engineering
Swansea University
Swansea SA2 8PP, UK
E-mail: mariolino.carta@swansea.ac.uk

O. Fuhr
Institute of Nanotechnology (INT) and Karlsruhe Nano Micro Facility (KNMFi)
Kaiserstraße 12, 76131 Karlsruhe, Germany

The ORCID identification number(s) for the author(s) of this article can be found under https://doi.org/10.1002/adfm.202401957

DOI: 10.1002/adfm.202401957

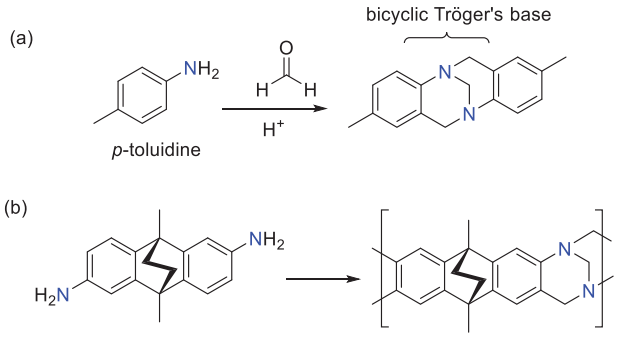

Scheme 1. a) Synthesis of a Tröger's base as exemplified by the reaction of *p*-toluidine with formaldehyde. b) Synthesis of a Tröger's base PIM from a bifunctional diamine monomer.

carbon dioxide from other gases. Their performance reached a level that they are now considered as the new state-of-the-art for gas separation membranes involving CO_2.[12] The exceptional properties of PIMs for this application arise from the combination of a very narrow pore size (typically between 3.5 and 8.5 Å)[13] that allows for excellent molecular sieving (CO_2 has a kinetic diameter of 3.3 Å), and a complete organic backbone that enhances their ability to "dissolve" CO_2 within the material.[14]

Another major advantage of PIMs lies in the extensive range of functional groups that can be incorporated into their monomers, either before polymerization[15] or introduced into the preformed backbone through post-polymerization methods.[16] This feature enables the precise tuning of their properties, constantly expanding the scope of their applications.[17] A specific example of this facile functionalization is represented by a recent subclass of PIMs that included in their backbones the so-called Tröger's base (TB-PIMs)[14a,18] This core combines the typical high surface area of PIMs with the presence of two bridgehead basic nitrogen, which facilitate applications in CO_2 separation[19] and heterogeneous catalysis.[11]

In general, the synthesis of the bicyclic TB entails the condensation reaction between an amine and an aldehyde under acidic conditions (**Scheme 1a**). Thus, for the preparation of a polymer, a symmetric bifunctional diamine monomer is imperative (Scheme 1b).

In this work, we describe the synthesis of TB PIMs containing PCPs, thus introducing innovative PCP-PIMs specifically designed for the efficient separation of carbon dioxide from nitrogen. The chemical structures of the monomers and the PIMs prepared are shown in **Figure 1** below.

2. Results and Discussion

2.1. Monomer Synthesis

The work commenced with the preparation of the amino-functionalized PCP monomers shown in Figure 1. The first step of the synthesis of monomers ***p*PCP-PA** and ***(rac)-m*PCP-PA** involves bromination of the [2.2]paracyclophane framework to form the brominated PCPs (exemplified by the pseudo-*para* monomer **1a** in **Scheme 2**; also see Scheme S1, Supporting Information). The brominated PCPs were then subjected to a Suzuki-type reaction with 4-(*N*-Boc-amino)phenylboronic acid **(2)** to form Boc-protected derivatives **3a** and **3b** (also see Scheme S2, Supporting Information), which could be purified via flash column chromatography to provide pure products in moderate-low yields, for example, **3a**: 44%, followed by deprotection with trifluoroacetic acid (TFA) in anhydrous methylene chloride.

The final monomers could be obtained in pure form in reasonable yields (60–80%) via crystallization of their acid salts followed by base-neutralization. A single crystal was obtained for ***p*PCP-PA** and its structure and characterization data can be found in the (see Section S7, Supporting Information). As expected, a single crystal revealed the planarity of ***p*PCP-PA**.

The synthesis of monomer ***p*PCP-DA** could be carried out in one step from **1a** by Hartwig-type coupling with NH_3, following a published procedure.[20] The pure product could be isolated using flash chromatography as a colourless solid with a 70% yield. Due to its instability in air (it is susceptible to oxidation[4b]), it was converted to the hydrochloride acid salt for storage and transportation and base-neutralized prior to usage.

2.2. Synthesis of Polymers

The starting point of the polymer synthesis was the polymerization of the simplest of the dianiline monomers, ***p*PCP-DA**, using typical TB formation conditions, for example, dimethoxy methane (DMM) as the crosslinker and trifluoroacetic acid (TFA) as the solvent and acid medium that is typically required for the TB formation, to form a model compound **PCP-TB** (**Scheme 3**).[14a,18] DCM was also added in this case to assist with solubilization of the monomer.

Because of the intrinsic instability and reactivity of the monomer, it was kept under an inert atmosphere and the polymerization was conducted under nitrogen, providing an insoluble black powder that hints at a high degree of cross-linking.

To improve the solubility and stability to oxidation of the materials of the monomer(s), we synthesized the extended monomers ***p*PCP-PA** and ***m*PCP-PA** and polymerized them separately under the same TB conditions but without DCM (Schemes S4 and S5, Supporting Information). We anticipated that the addition of the extra aromatic moiety would enhance the solubility of the monomers and polymer for two reasons: 1) by adding an extra organic component, the overall solubility in organic solvents is normally improved; 2) by adding an extra free-rotation site, the overall rigidity diminishes.

2.3. Polymer Characterization

2.3.1. Structure Characterization

Even though **PCP-TB** was insoluble, a full characterization of the polymer demonstrated that the TB cores had formed efficiently. **Figure 2a** shows a MALDI–TOF spectrum of the volatile low molecular mass fraction, obtained from the washing out of short oligomers during the polymer's workup (see Section S13.3, Supporting Information), which shows a clear pattern of repeated units (M ≈ 275 Daltons). We believe that the extra repeating peaks of Figure 2a belong to the trifluoroacetate that acts as the counteranion of each protonated TB nitrogen. The formation of

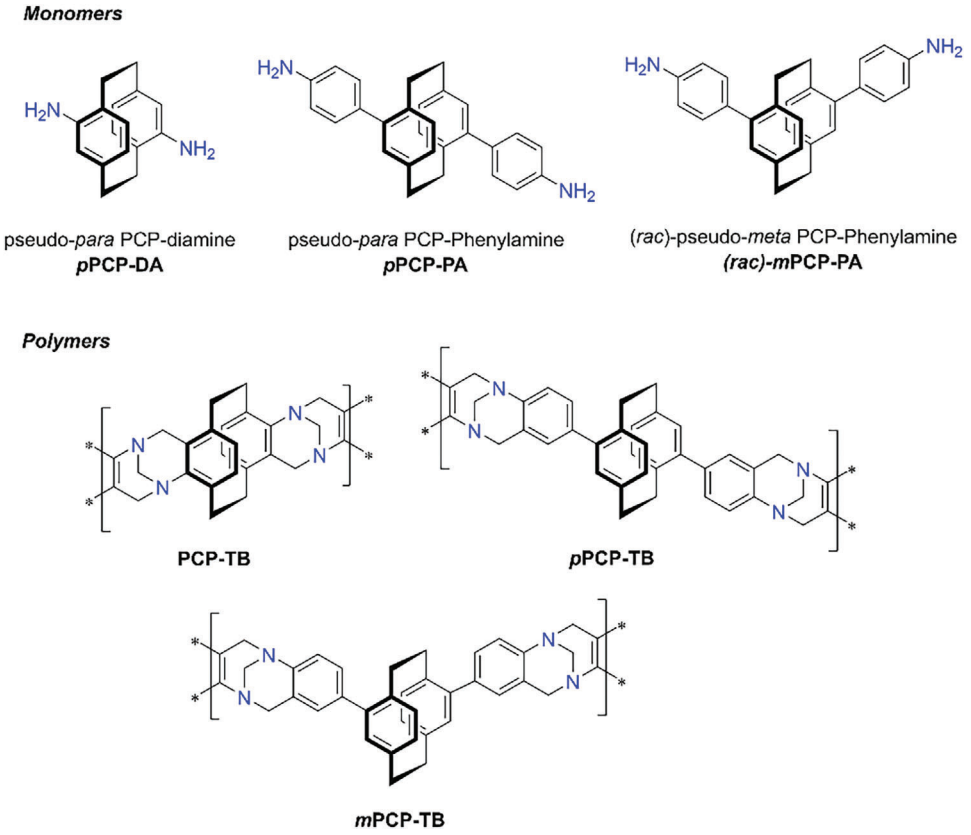

Figure 1. Chemical structures of the monomers and polymers presented in this work.

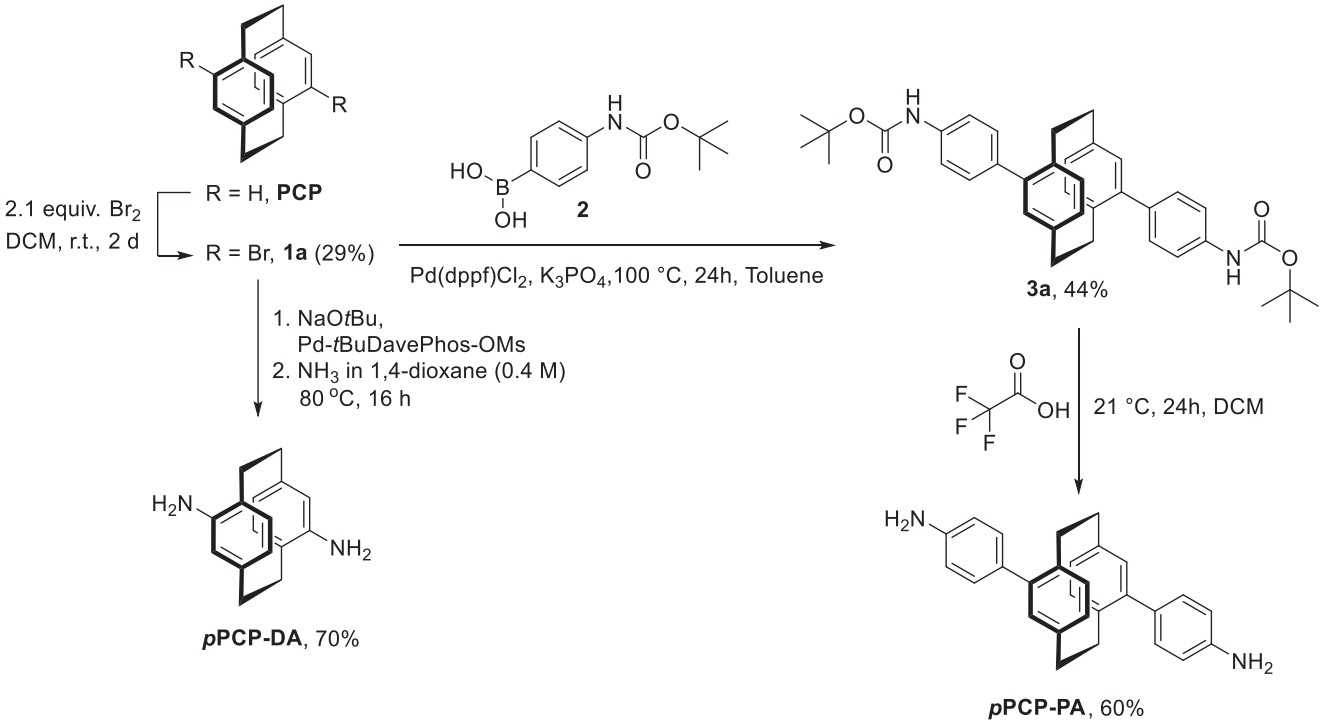

Scheme 2. Synthesis of monomers ***p*PCP-DA** and ***p*PCP-PA** commencing with **PCP** and dibrominated **PCP** (**1a**).

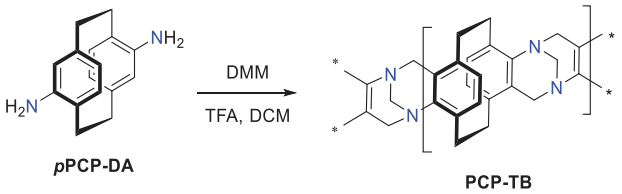

Scheme 3. Synthesis of polymer **PCP-TB** from monomer ***p*PCP-DA**.

the "extended" pseudo-*para* and pseudo-*meta* polymers, namely ***p*PCP-TB** and ***m*PCP-TB**, proceeded more smoothly, due to the enhanced stability shown by the corresponding dianilines toward oxidation in air. The two polymers also exhibited a lighter colour compared to **PCP-TB** (as anticipated for TB polymers), and both showed the characteristic features of TB, thereby confirming the efficacy of the reaction. A ^{15}N solid-state NMR experiment suggests the presence of a single species of nitrogen (Figure 2b),[21] while analysis of the solid-state ^{13}C NMR spectrum of the ***m*PCP-TB** exhibited the typical three peaks ≈70–50 ppm that are signature of the TB core (Figure 2c).[11]

As anticipated, the solubility of the materials varied depending on the starting monomer. The polymer obtained from the simplest **PCP-DA** gave a poorly soluble material, whereas the two extended versions demonstrated good solubility in chloroform which is typical of TB-PIMs. Furthermore, the pseudo-*meta* polymer (***m*PCP-TB**) demonstrated improved solubility compared to its pseudo-*para* counterpart (***p*PCP-TB**) which may be attributed to the relatively more "linear" structure of the pseudo-*para* form which results in a denser and less soluble material. The pseudo-*meta* configuration, with its more contorted nature, exhibited a solubility in chloroform that enabled its characterization using solution ^1H NMR (Figure S1, Supporting Information). FT-IR spectra also confirmed the efficient formation of the TB core (Figures S10–S12, Supporting Information) with the evident peaks of the C–N stretch visible ≈1300–1200 cm^{-1}, supported by previously reported examples.[22]

2.3.2. Textural Properties

All polymers were characterized in terms of porosity, thermal stability, and CO_2/N_2 selectivity - estimated using Ideal Absorbed Solution Theory (IAST). **Table 1** summarizes the main textural properties discussed below. Specifically, the Bet values, the CO_2 adsorptions at different temperatures, the (CO_2/N_2) IAST selectivity, and the isosteric heats of adsorption (crucial to assess the affinity of the materials toward CO_2). The adsorption of N_2 for all three polymers at 77 K did not show good porosity (Figure S15, Supporting Information), which came as a surprise as both PCP- and TB- based materials previously proved to be porous.[4b,18,23] However, looking at the unexpected "flatness" of the XRD crystal structure of the extended *p*PCP monomer (Figure S21, Supporting Information), we presume that the polymer probably packs in the solid-state better than we anticipated, with a consequent loss of porosity. The lack of substantial porosity, when measured by N_2 adsorption at very low temperatures, could be attributed to a relatively efficient packing of the polymer chains, which limits the diffusion of this probe gas.[24] For this reason, we also assessed the BET surface areas (SA_{BET}) of these new materials via isothermal CO_2 adsorption at 273 K, known to provide comparable results with N_2 in the past (Figure S17, Supporting Information).[11,25] Indeed, the data from this measurement showed an increased porosity for CO_2 compared to the N_2 assessment. Table 1 shows that the SA_{BET} increases in the order ***p*PCP-TB** > ***m*PCP-TB**~**PCP-TB**, which is obviously the same order as the single CO_2 uptakes at 273 K (**Figure 3a**). Pore size distribution, also assessed from CO_2 adsorption and calculated using Non-Local Density Functional Theory (NLDFT),[26] shows that all the PCP-based materials present very similar pore sizes (Figure 3b).

Thermogravimetric analysis (TGA) showed the typical high thermal stability of PIMs, with decomposition temperatures between 435 and 460 °C and char yields between 53% and 63% (Figure S8, Supporting Information). The higher decomposition temperatures of the two extended versions suggest a slightly higher degree of polymerization. Gel permeation chromatography (GPC) was also attempted to estimate the molecular mass of the soluble polymers; however, the results are not conclusive as only very faint peaks were observed. We attributed this problem to the fact that often the basic TB cores cause the polymer to block the column because of their interaction with the slightly acidic chloroform mobile phase.

2.3.3. Morphology of the TB Polymers

The macroporous nature of the surface of the polymers was confirmed using Scanning Electron Microscopy (SEM) (Figures S19 and S20, Supporting Information). Some parts of the samples showed semi-regular pore arrangements with pore diameters ≤

Table 1. Textural properties of PCP-TB polymers.

Polymer	$SA_{BET, CO2}$ [a] [$m^2\ g^{-1}$]	$V_{ADS, CO2}$ [b] [$cm^3\ g^{-1}$] [$mmol\ g^{-1}$]	$V_{ADS, CO2}$ [c] [$cm^3\ g^{-1}$] [$mmol\ g^{-1}$]	Q_{ST} [d] [$kJ\ mol^{-1}$]	CO_2/N_2 [e] (IAST)
PCP-TB	197	18.7 [0.835]	15.7 [0.701]	27.8	69.4
***m*PCP-TB**	208	23.7 [1.06]	15.1 [0.673]	28.7	56.8
***p*PCP-TB**	233	29.8 [1.325]	13.8 [0.616]	32.6	47.5

[a] BET surface areas (SA_{BET}) calculated for CO_2 at 273K over the P/P_0 range 0.01–0.1; [b] CO_2 uptake at 273 and 298 K, respectively (1 bar); [c] CO_2 uptake at 273 and 298 K, respectively (1 bar); [d] Isosteric heat of adsorption (in kJ mol−1) of corresponding gas at zero coverage calculated from isotherms collected at 273 and 298 K and fitted with the Langmuir–Freundlich equation and calculated via the Clausius Clapeyron equation; [e] selectivity of CO_2 over N_2 adsorption (IAST, 298 K for a CO_2/N_2 15/85 composition.

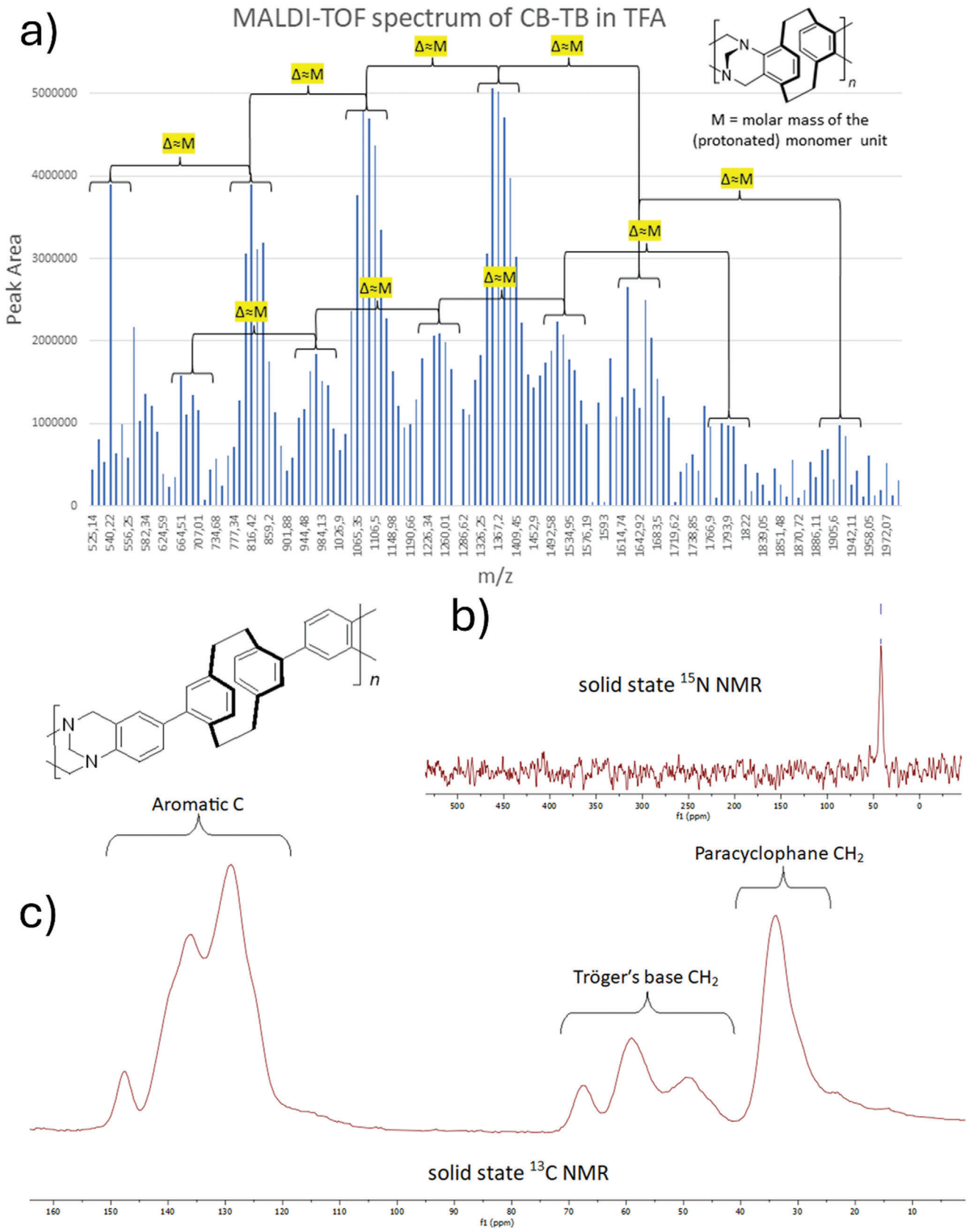

Figure 2. Characterisation of PCP-TB polymers. a) MALDI-TOF spectrum of repeated units of **PCP-TB**; b) ^{15}N Solid-state NMR and c) ^{13}C Solid-state NMR of ***p*PCP-PA**.

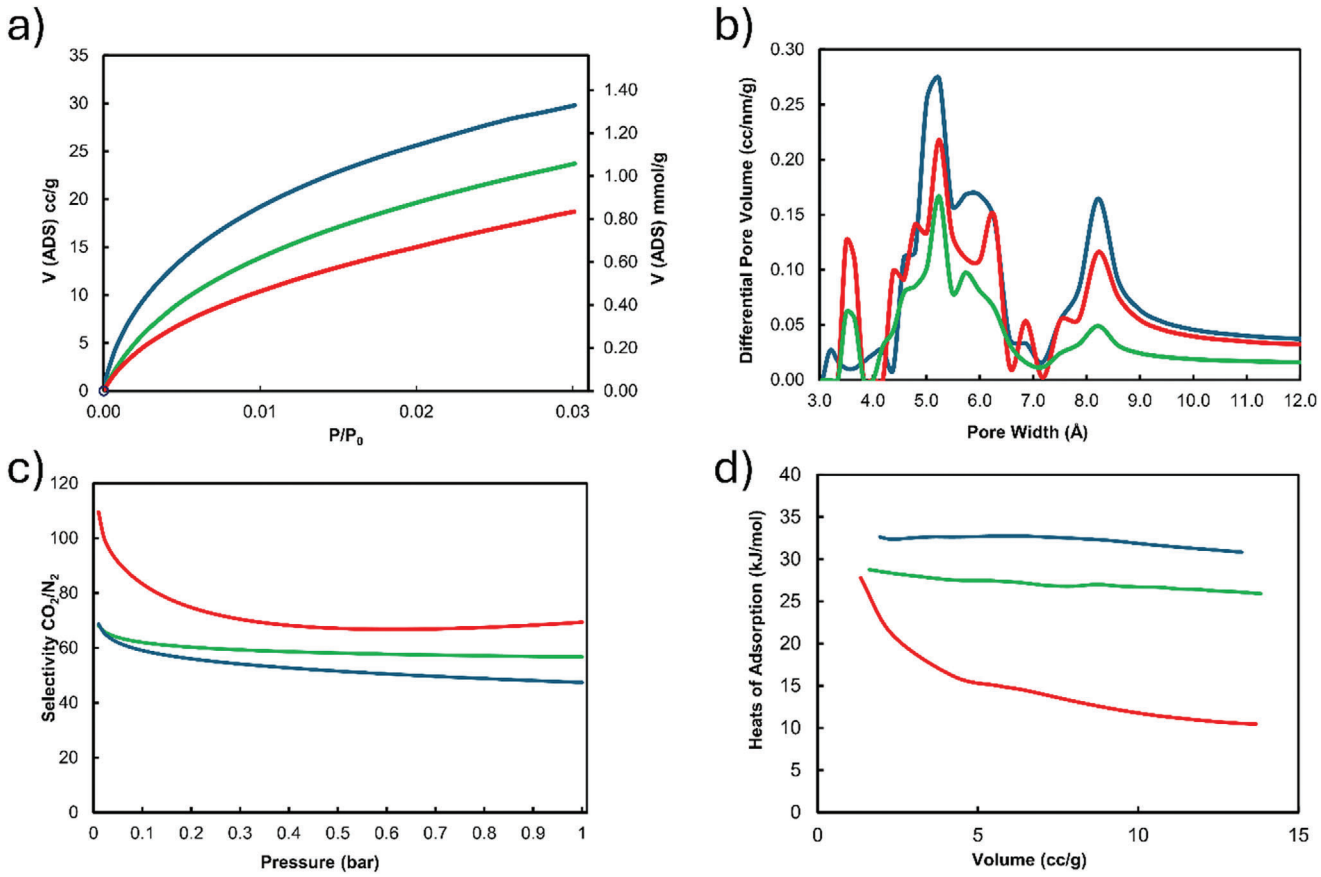

Figure 3. a) CO_2 adsorption isotherms measured at 273 K [blue (***p*PCP-TB**), green (***m*PCP-TB**), red (**PCP-TB**) (desorption curves were removed for clarity, details are available in S.I.); b) NLDFT pore size distribution (PSD), calculated from CO_2 at 273K; c) IAST CO_2/N_2 ideal selectivity for a mixture 15/85; (d) Isosteric heats of adsorption of PCP-TB polymers.

1 µm. ***p*PCP-TB** seemed to have the largest number of pores. Some samples also showed particles with diameters below 1 µm diameter. The smallest particles were ≈20 nm in diameter.

2.3.4. CO_2/N_2 Selectivity

Considering the final CO_2 uptakes, it could be asserted that the adsorptions are not particularly high (29.7–18.7 cc g^{-1} or 1.325–0.835 mmol g^{-1}), especially if we foresee the use of these materials for general carbon capture (i.e., simple adsorption of CO_2).[26,27] However, when the same CO_2 adsorption measurements are conducted at 25 °C (298 K), the temperature at which the separation of CO_2 from N_2 from flue gas is typically performed, the results are very different and more interesting, as we discovered a trend inversion of the CO_2 adsorptions.

Despite the lower CO_2 uptakes at this temperature compared to those reported at 273 K (15.7–13.8 cc g^{-1} or 0.701–0.616 mmol g^{-1} at 298 K, Table 1), it must be emphasized that the impact of material for CO_2 adsorption extends well beyond the final gas uptake. The efficacy of a gas separation material lies in its ability to effectively separate one gas (e.g., CO_2) from other gases, particularly nitrogen. Indeed, one of the most crucial applications of carbon capture involves the separation of CO_2 from N_2 which, in a 15:85 ratio, represents the typical composition of flue gas and it is ideally conducted at 298 K, mimicking vacuum swing adsorption conditions (VSA).[28]

Even more intriguingly, at this temperature, the order of CO_2 uptakes is as follows: **PCP-TB > *m*PCP-TB > *p*PCP-TB**, essentially reversing the uptake sequence at 273 K. This could be attributed to the more rigid nature of **PCP-TB**, which can keep adsorbing CO_2 even at a higher temperature, whereas the pores of the more "flexible" pseudo-*meta* and pseudo-*para* counterparts are partly blocked. This claim is further confirmed by closely analyzing the pore size distribution of Figure 3b, which shows that **PCP-TB** possesses a higher amount of ultra-micropores centered at ≈3.5 Å. Even though PSD assessed via gas adsorption is merely qualitative,[24] its use to assess very similar polymers in the same isothermal conditions can be deemed as very reliable in evaluating trends.[24] This inversion of uptakes for CO_2 is also combined with a very low adsorption of N_2 at 298 K (Figure S18, Supporting Information). This outcome is in line with expectations, as even at 77 K the adsorption of nitrogen proved to be rather low. This resulted in a higher CO_2/N_2 selectivity for **PCP-TB** (≈70, Table 1 and Figure 3c) compared to the extended versions (≈57 for ***m*PCP-TB** and ≈47 for ***p*PCP-TB**), which still represent relatively high selectivity for these categories of adsorbents. Our results are in line with or superior to previously

published polymers with similar surface areas, CO_2 uptake, and CO_2/N_2 selectivity, especially when comparing polymers that contain nitrogen in their backbones. For instance, Saleh et al reported a hypercrosslinked polymer that includes indoles as the main monomer, with a BET surface area of 243 m^2g^{-1} combined with a CO_2/N_2 selectivity of 66 at 298 K and 1 bar.[29] Chola and co-workers showed a carbazole-based polymer with 338 m^2g^{-1} and selectivity 53 at 298 K and 1 bar.[30] Xu and Hedin reported the synthesis and characterization of a series of microporous organic polymers (MOPs) with BET surface areas from 70 to 589 m^2g^{-1} and CO_2/N_2 selectivities between 77 and 65.[31]

Finally, an evaluation of the heats of adsorption (Q_{st}, Table 1 and Figure 3d), which is indicative of the potential chemical affinity for CO_2, reveals that our materials fall within the physisorption range (≈28–32 kJ mol^{-1}), suggests that CO_2 is not strongly bonded to the polymer. Existing research shows that Q_{st} values within the range of chemisorption (which implies a strong chemical affinity of the material for the gas), become significant only beyond 50 kJ mol^{-1}. This means that in our case the gas is only "mechanically" trapped within the pores, as the energy of physisorption is comparable to van der Waals forces.[32] This feature becomes highly significant when considering that desorption of CO_2 in carbon capture should not incur with an energy penalty (as would be the case with chemisorption). Therefore, we can assert that our materials do not need additional pressure or temperature to facilitate the desorption of CO_2, which is highly advantageous. The shape of the Q_{st} curves displayed by the TB polymers is slightly different. The two extended pseudo-*meta* and pseudo-*para* TBs, which possess extra free rotation sites compared to PCP-TB, show rather "flat" trends where the Q_{st} does not change significantly with the increase of the volume adsorbed. For PCP-TB, instead, it seems that the Q_{st} decreases rapidly. Our hypothesis is that PCP-TB, which shows the highest V(ADS) at 298 K (Table 1), has its pores filled with CO_2 more quickly than the others, which also translates into an enhanced IAST selectivity. The lower overall Q_{st} of PCP-TB is likely attributed to this superior physisorption mechanism (it is more molecular sieving), which rapidly reduces the affinity for CO_2 when the pores get filled with the gas. The lower the affinity for CO_2, the more rapidly the Q_{st} is reduced. This trend is common in many other polymers.[33]

3. Conclusion

We developed a series of novel PIMs based on the combination of TB and PCP cores. The chosen monomers varied in size from the diamino PCP, to two "extended" versions that contain an extra aromatic moiety and a site of free rotation. The monomers and polymers were extensively characterized with different techniques, assessing their structures by NMR (both in solution and the solid-state), FT-IR, BET, PSD, and SEM. Porosity assessment shows lower BET surface areas than expected from the combination of these two cores, however, the relative lack of porosity was counterbalanced by a high selectivity toward the separation CO_2/N_2 (15/85), critical for carbon capture and sequestration of CO_2 from flue gas. The smaller PCP-TB demonstrated higher selectivity values than the correspondent extended versions, showing that the vicinity of the TB and PCP cores played a significant role in the separation of these two gases. All polymers possessed low heats of adsorption, meaning that the CO_2 will be trapped primarily "mechanically" rather than chemically. This feature is advantageous, as the release (desorption) of the gases would not require substantial energy inputs, such as heat or vacuum. Along with the pleasing results regarding gas separation, we foresee the use of these PCP-TB polymers in applications such as catalysis, electrochemistry, and chiral separations.

Supporting Information

Supporting Information is available from the Wiley Online Library or from the author.

Acknowledgements

Y.L. receives funding from CSC scholarship 202208080097. J.B. thanks the Carl Zeiss Foundation for financial support and acknowledges funding by the Deutsche Forschungsgemeinschaft (DFG, German Research Foundation) under Germany's Excellence Strategy – 2082/1 – 390761711. RJvV acknowledges the Slovenian Innovation and Research Agency (ARIS) for funding (Project No. J7-50041). R.D.Jv.V. and M.J. acknowledge ARIS for funding under the Research Core Funding Grant P1-0230, and the authors thank Mr. Blaž Kisovec for technical assistance during the synthesis of the monomers. M.C. and Y.W. gratefully acknowledge funding from the Engineering and Physical Sciences Research Council (EPSRC), Grant number: EP/T007362/1 "Novel polymers of intrinsic microporosity for heterogeneous base-catalyzed reactions (HBC-PIMs)" and Swansea University. A.Z. acknowledges the Magnus Ehrnrooth Foundation for financial support. The authors acknowledge the financial support of the University of Helsinki and the use of ALD center Finland research infrastructure.

Open access funding enabled and organized by Projekt DEAL.

Conflict of Interest

The authors declare no conflict of interest.

Data Availability Statement

The data that support the findings of this study are available on request from the corresponding author. The data are not publicly available due to privacy or ethical restrictions.

Keywords

gas sorption, paracyclophanes, PIMs, polymers, porosity, Tröger's base

Received: January 31, 2024
Revised: April 14, 2024
Published online:

[1] M. L. Birsa, H. Hopf, P. G. Jones, L. G. Sarbu, L. G. Bahrin, *Materials* **2023**, *16*, 4051.
[2] C. Liao, Y. Zhang, S. H. Ye, W. H. Zheng, *ACS Appl. Mater. Interfaces* **2021**, *13*, 25186.
[3] a) E. Elacqua, T. Friščić, L. R. MacGillivray, *Isr. J. Chem.* **2012**, *52*, 53; b) W. Gong, H. Xie, K. B. Idrees, F. A. Son, Z. Chen, F. Sha, Y. Liu, Y. Cui, O. K. Farha, *J. Am. Chem. Soc.* **2022**, *144*, 1826.
[4] a) H. Hopf, *Angew. Chem., Int. Ed.* **2008**, *47*, 9808; b) L. J. Huang, Y. T. Weng, A. Raiz, Z. J. Mao, X. H. Ma, *Chin. J. Polym. Sci.* **2023**, *41*, 1617; c) Y. Morisaki, Y. Chujo, *Prog. Polym. Sci.* **2008**, *33*, 346; d) H. Maeda, R. Inoue, A. Saeki, Y. Morisaki, *Polym. J.* **2023**, *55*, 537.

[5] N. B. McKeown, *Polymer* **2020**, *202*, 122736.
[6] N. B. McKeown, *Sci. China: Chem.* **2017**, *60*, 1023.
[7] a) M. Tamaddondar, A. B. Foster, M. Carta, P. Gorgojo, N. B. McKeown, P. M. Budd, *ACS Appl. Mater. Interfaces* **2020**, *12*, 46756; b) B. Qiu, M. Yu, J. M. Luque-Alled, S. Ding, A. B. Foster, P. M. Budd, X. Fan, P. Gorgojo, *Angew. Chem., Int. Ed.* **2024**, *63*, e202316356.
[8] C. Pathak, A. Gogoi, A. Devi, S. Seth, *Chem. Eur. J.* **2023**, *29*, e202301512.
[9] F. Marken, M. Carta, N. B. McKeown, *Anal. Chem.* **2021**, *93*, 1213.
[10] a) E. Al-Hetlani, M. O. Amin, A. R. Antonangelo, H. Zhou, M. Carta, *Microporous Mesoporous Mater.* **2022**, *330*, 111602; b) Z. Li, J. P. Lowe, P. J. Fletcher, M. Carta, N. B. McKeown, F. Marken, *ACS Appl. Mater. Interfaces* **2023**, *15*, 42369.
[11] A. R. Antonangelo, N. Hawkins, E. Tocci, C. Muzzi, A. Fuoco, M. Carta, *J. Am. Chem. Soc.* **2022**, *144*, 15581.
[12] B. Comesaña-Gándara, J. Chen, C. G. Bezzu, M. Carta, I. Rose, M. C. Ferrari, E. Esposito, A. Fuoco, J. C. Jansen, N. B. McKeown, *Energy Environ. Sci.* **2019**, *12*, 2733.
[13] C. H. Lau, K. Konstas, C. M. Doherty, S. J. Smith, R. Hou, H. Wang, M. Carta, H. Yoon, J. Park, B. D. Freeman, *Nanoscale* **2020**, *12*, 17405.
[14] a) M. Carta, R. Malpass-Evans, M. Croad, Y. Rogan, J. C. Jansen, P. Bernardo, F. Bazzarelli, N. B. McKeown, *Science* **2013**, *339*, 303; b) Y. Wang, B. S. Ghanem, Z. Ali, K. Hazazi, Y. Han, I. Pinnau, *Small Structures* **2021**, *2*, 2100049; c) D. M. D'Alessandro, B. Smit, J. R. Long, *Angew. Chem., Int. Ed.* **2010**, *49*, 6058.
[15] S. A. Felemban, C. G. Bezzu, B. Comesaña-Gándara, J. C. Jansen, A. Fuoco, E. Esposito, M. Carta, N. B. McKeown, *J. Mater. Chem. A* **2021**, *9*, 2840.
[16] a) Q. Xu, J. Jiang, *J. Membr. Sci.* **2019**, *591*, 117357; b) H. Zhou, C. Rayer, A. R. Antonangelo, N. Hawkins, M. Carta, *ACS Appl. Mater. Interfaces* **2022**, *14*, 20997.
[17] M. L. Jue, R. P. Lively, *Curr. Opin. Chem. Eng.* **2022**, *35*, 100750.
[18] M. Carta, R. Malpass-Evans, M. Croad, Y. Rogan, M. Lee, I. Rose, N. B. McKeown, *Polym. Chem.* **2014**, *5*, 5267.
[19] Q. Xu, B. Xin, J. Wei, Y. Ma, Z. Qing, C. Feng, S. Yi, N. Li, K. Li, F. Wang, J. Zhao, L. Yang, L. Yao, W. Jiang, Y. Dai, Z. Dai, *J. Mater. Chem. A* **2023**, *11*, 15600.
[20] S. L. Buchwald, W. Huang, US 2016035911A1, **2016**.
[21] C. Hu, Q. Zhang, C. Lin, Z. Lin, L. Li, F. Soyekwo, A. Zhu, Q. Liu, *J. Mater. Chem. A* **2018**, *6*, 13302.
[22] J. Byun, S. H. Je, H. A. Patel, A. Coskun, C. T. Yavuz, *J. Mater. Chem. A* **2014**, *2*, 12507.
[23] V. Kumar, S. Chatterjee, P. Sharma, S. Chakrabarty, C. V. Avadhani, S. Sivaram, *J. Polym. Sci., Part A. Polym. Chem.* **2018**, *56*, 1046.
[24] D. Lozano-Castelló, D. Cazorla-Amorós, A. Linares-Solano, *Carbon* **2004**, *42*, 1233.
[25] S. L. Cognata, R. Mobili, C. Milanese, M. Boiocchi, M. Gaboardi, D. Armentano, J. C. Jansen, M. Monteleone, A. R. Antonangelo, M. Carta, V. Amendola, *Chem. Eur. J.* **2022**, *28*, e202201631.
[26] K. A. Cychosz, M. Thommes, *Engineering* **2018**, *4*, 559.
[27] R. L. Siegelman, E. J. Kim, J. R. Long, *Nat. Mater.* **2021**, *20*, 1060.
[28] a) H. Zhang, Z. Zhou, Y. Yin, H. Xu, Y. Wang, K. Yang, Z. Zhang, J. Wang, X. He, *EcoEnergy* **2023**, *1*, 217; b) M. Chawla, H. Saulat, M. Masood Khan, M. Mahmood Khan, S. Rafiq, L. Cheng, T. Iqbal, M. I. Rasheed, M. Z. Farooq, M. Saeed, N. M. Ahmad, M. B. Khan Niazi, S. Saqib, F. Jamil, A. Mukhtar, N. Muhammad, *Chem. Eng. Technol.* **2020**, *43*, 184; c) K. A. Fayemiwo, G. T. Vladisavljević, S. A. Nabavi, B. Benyahia, D. P. Hanak, K. N. Loponov, V. Manović, *Chem. Eng. J.* **2018**, *334*, 2004,. d) A. Ntiamoah, J. Ling, P. Xiao, P. A. Webley, Y. Zhai, *Adsorption* **2015**, *21*, 509.
[29] M. Saleh, H. M. Lee, K. C. Kemp, K. S. Kim, *ACS Appl. Mater. Interfaces* **2014**, *6*, 7325.
[30] N. Merukan Chola, P. Gajera, H. Kulkarni, G. Kumar, R. Parmar, R. K. Nagarale, G. Sethia, *ACS Omega* **2023**, *8*, 24761.
[31] C. Xu, N. Hedin, *J. Mater. Chem. A* **2013**, *1*, 3406.
[32] L. W. Bruch, *Surf. Sci.* **1983**, *125*, 194.
[33] a) K. A. Fayemiwo, N. Chiarasumran, S. A. Nabavi, V. Manović, B. Benyahia, G. T. Vladisavljević, *J. Environ. Chem. Eng.* **2020**, *8*, 103536; b) H. Hong, Z. Guo, D. Yan, H. Zhan, *Microporous Mesoporous Mater.* **2020**, *294*, 109870.